Figure S1

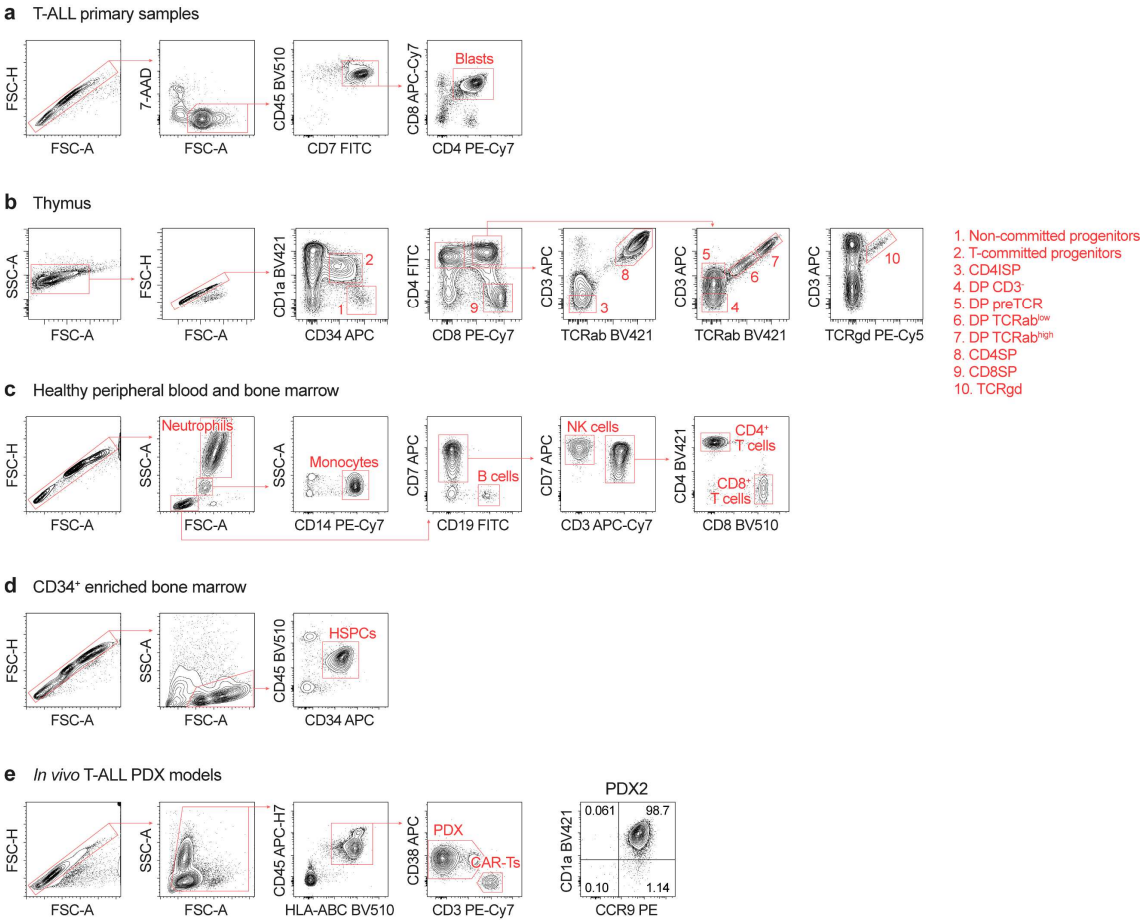

Suppl Fig1. Gating strategies for flow cytometry analyses. (**a**) Flow cytometry gating strategies for T-ALL primary samples. Blasts were identified as $CD7^{+}CD45^{dim}$ and were further gated based on CD4 and CD8 expression to exclude healthy (single $CD4^{+}$ and single $CD8^{+}$) T cells from the analysis. (**b-d**) Flow cytometry gating strategies for the indicated cell populations within healthy thymus (**b**), PB and total BM (**c**), and MACS-enriched BM $CD34^{+}$ HSPCs (**d**). (**e**) Flow cytometry gating strategies for *in vivo* PDX assays. A representative phenotype of PDX2 is included.

Figure S2

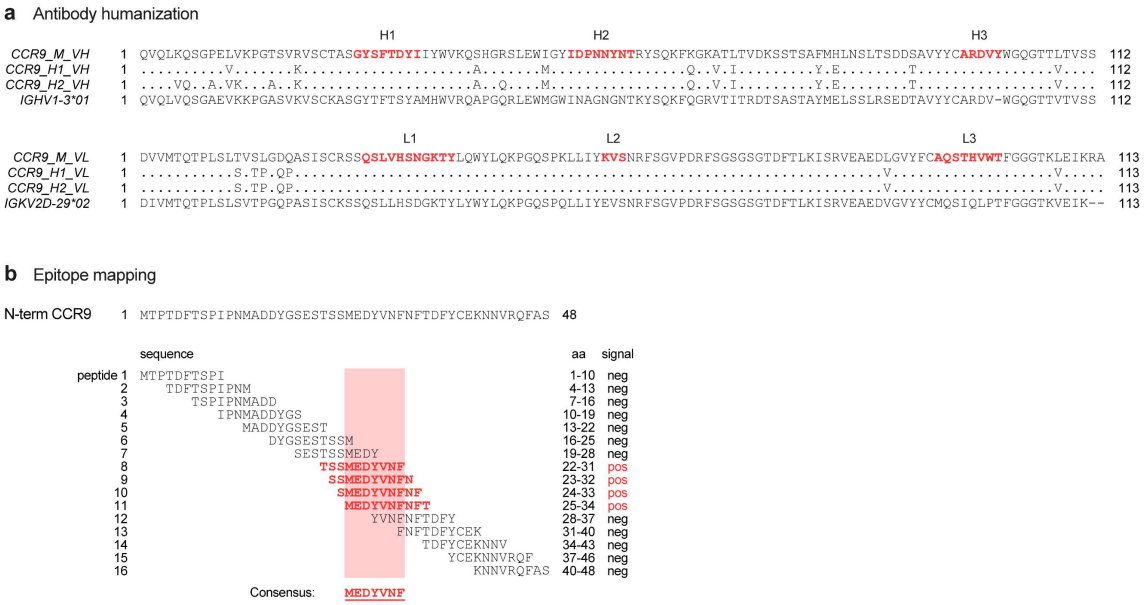

Suppl Fig2. CCR9 binder characterization. (**a**) Protein sequence alignment of the original murine heavy (V_H) and light (V_L) chains with their humanized counterparts (H1 and H2) and the most structurally similar human immunoglobulin gene. CDRs are highlighted in red, and only mutated residues in the humanized sequences are shown. (**b**) Epitope mapping of the anti-CCR9 binder. Overlapping peptides were derived from the extracellular N-terminus tail of CCR9 and tested for binding to recombinant anti-CCR9 H2 scFv by ELISA (ProteoGenix). The consensus sequence is indicated.

Figure S3

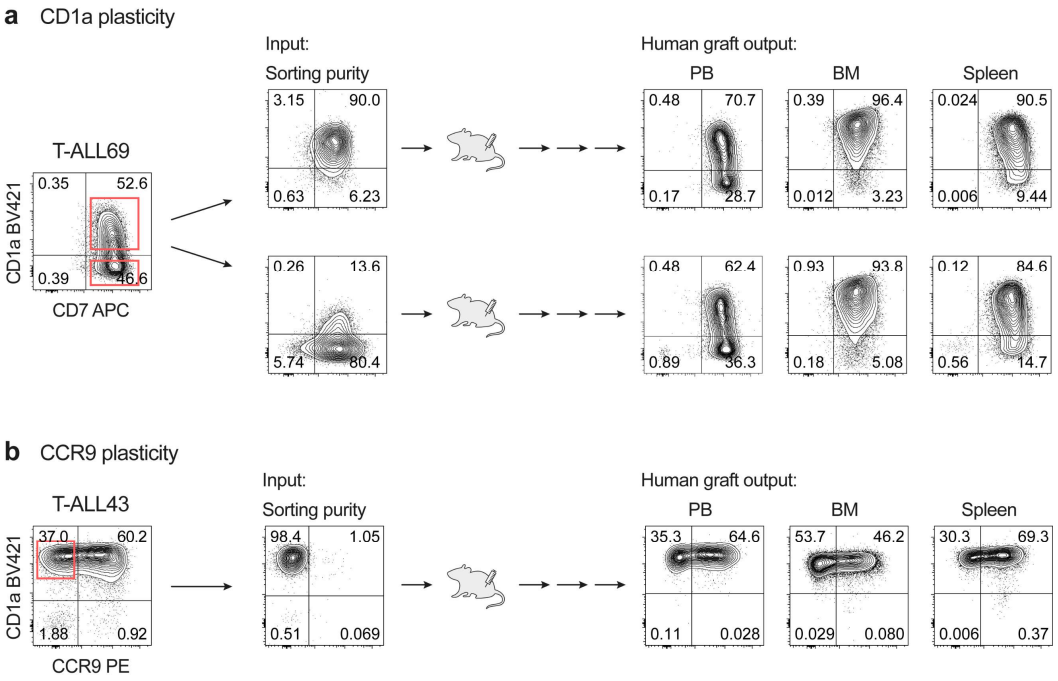

Suppl Fig3. Expression plasticity of CD1a and CCR9. Two primary T-ALL samples with variable expression of CD1a (**a**) and CCR9 (**b**) were sorted, and the purified CD1a$^{+/-}$ or CCR9^{-} fractions (purity: 81-98%) were transplanted into NSG mice. Leukemic grafts were followed up biweekly and mice were sacrificed for leukemia immunophenotyping upon graft detection in PB.

Figure S4

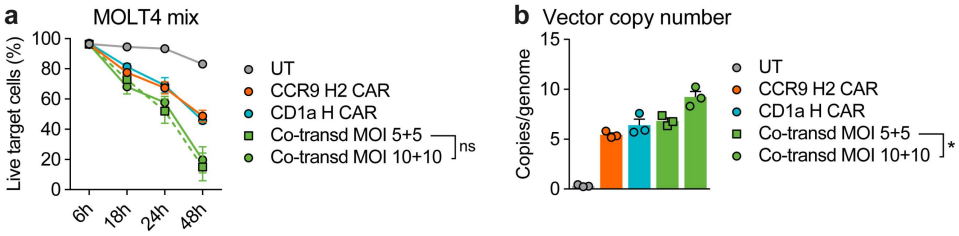

Suppl Fig4. Impact of MOI in co-transduced dual CAR-T cell assays. (**a**) Time-course cytotoxicity comparing co-transduced dual CAR-T cells using a MOI of 5 *versus* 10 for each CAR against mixed target cells at a 1:1 E:T ratio (*n*=3), as described in Fig. 5a. (**b**) Vector copy number (VCN) in co-transduced dual CAR-T cells using a MOI of 5 *versus* 10 for each CAR (*n*=3).

Figure S5

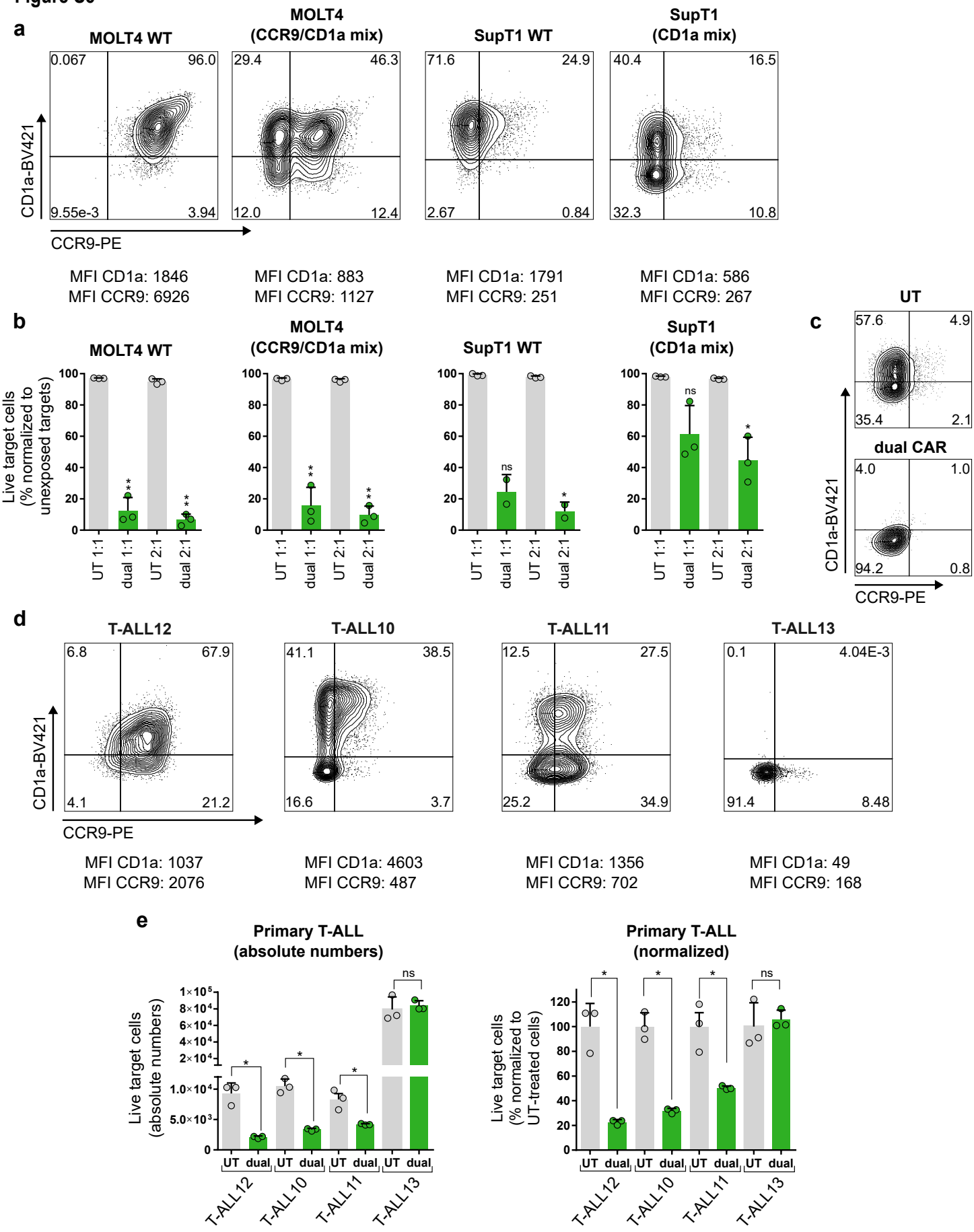

Suppl Fig5. Efficacy of CCR9/CD1a dual CAR-T cells against cell lines and primary cells with phenotypically heterogeneous CCR9/CD1a populations. (**a**) Contour plots showing the level of CCR9 and CD1a in T-ALL cell lines before (WT) and after partial genomic KO of CCR9 and/or CD1a. The number in each quadrant shows the percentage of cells. MFI values for CCR9 and CD1a antibodies are presented below each plot. (**b**) Cytotoxicity of CCR9/CD1a dual CAR-T cells against T-ALL cells was assessed by flow cytometry. Target cells were pre-stained with eFluor 670 dye and exposed to UT or dual CAR-T cells for 48h at the indicated E:T ratios. The bars show the percentage of eFluor670^{+}7AAD^{-} cells normalized to

untreated target cells (n=3). Plots show mean + SD. P values were calculated using paired t-test (*p<0.05; **p<0.01, ns, not significant). (**c**) Contour plots showing CD1a and CCR9 levels in SupT1-CD1a mix cells following UT and dual CAR-T cell treatment. (**d**) Contour plots depicting the level of CCR9 and CD1a in selected primary T-ALL. The numbers on each plot indicate the percentage of antigen-positive cells. MFI values for CCR9 and CD1a antibodies are given below each plot. (**e**) Cytotoxicity of CCR9/CD1a dual CAR-T cells against T-ALL was assessed by flow cytometry. Target cells were pre-stained with eFluor 670 dye and exposed to either UT or dual CAR-T cells for 24h at 2:1 E:T ratio. The left panel shows the absolute number of residual live target cell population ($eFluor^{+}7AAD^{-}$) as determined by Trucount tubes. Plots show mean + SD (n=3). P values were calculated using paired t-test (*p<0.05; ns, not significant). The right panel shows the percentage of live cells normalized to UT T cell treatment.